Temperature dependence of the photoluminescence spectra from InAs(P)/InP multilayers containing thick quantum dots: Dot-size-dependent carrier dynamics

A. Lévesque,[1] P. Desjardins,[1] R. Leonelli,[2] and R. A. Masut[1]

[1]*Département de Génie Physique and Regroupement Québécois sur les Matériaux de Pointe (RQMP), École Polytechnique de Montréal, Case Postale 6079, Succursale Centre-Ville, Montréal, Québec, Canada H3C 3A7*

[2]*Département de Physique and Regroupement Québécois sur les Matériaux de Pointe (RQMP), Université de Montréal, Case Postale 6128, Succursale Centre-ville, Montréal, Québec, Canada H3C 3J7*

(Received 4 June 2010; revised manuscript received 4 April 2011; published 6 June 2011)

We have studied the temperature dependence (∼10–293 K) of the photoluminescence (PL) from InAs/InP(001) quantum dot (QD) multilayers with thin spacer layers (∼5 nm) emitting in the 0.6–0.8 eV spectral region. The QD emission redshifts less than the InAs bulk material band gap with increasing temperature. This behavior is accompanied by an important rise of the relative PL intensity of the higher-energy contributions to the spectra. The room-temperature emission is rather strong—over 20% of the low-temperature value—since deep confinement effects prevent the thermal escape of the carriers out of these relatively large QD's. In addition, the carrier transfer from the wetting layers to the QD's increases with the number of layers at low temperatures. A dot-size-dependent analysis of the carrier dynamics using a rate-equation model leads to the following interpretation of our experimental results: (i) the radiative emission intensity from thicker dots quenches at lower temperature through thermalization to excited nearly dark states, and (ii) carriers initially captured by the wetting layer are preferentially transferred to thinner QD's whose emission energy is higher than ∼0.7 eV. In multilayers, the experimental observations can be explained without involving electronic coupling between QD's of different layers, even though the distance between the vertically aligned nanostructures is small.

DOI: 10.1103/PhysRevB.83.235304 PACS number(s): 78.67.Hc, 73.21.La

I. INTRODUCTION

Understanding the temperature dependence of the optical properties of quantum dot (QD) structures is of crucial importance for their utilization in emitter devices. There have been several studies on this subject for the InAs/GaAs system.[1–6] While the latter can be regarded as a model system to understand the behavior of inhomogeneous ensembles of Stranski-Krastanov (SK) QD's, its optical properties can differ greatly from that of a system such as InAs/InP, where a smaller lattice mismatch (3.2%) can allow for a rich variety of nanostructures of different shapes and size distributions as well as more deeply confined carriers. In fact, SK-grown InAs nano-islands embedded in InP(001) have shown optical emission spectra covering a wide photon-energy range, depending on the quantity of material deposited and on the duration of the growth interruption time during which island formation takes place.[7–11] Indeed, one can observe emission from well-defined peaks, each associated to a family of thin dots of the same heights, in the 0.8–1.1 eV energy range,[9,11] while emission from thicker dots in the 0.6–0.8 eV region rather results in broader peaks[8,10] with an indiscernible contribution from the different families, since the energy separation between two successive families decreases as the thickness of the dots is increased. In the latter case, the carriers are deeply confined, so a more stable emission behavior with temperature can be expected from such nanostructures, as compared with InAs/GaAs or thinner InAs/InP QD's.

For InAs/GaAs QD samples, the energy of the emission peak from the QD's has been shown to shift faster with temperature than the bulk InAs band gap,[1–4,6] this redshift being smaller for samples with larger dots.[4,6] Fafard *et al.*[1] have shown, however, that the temperature dependence of the emission from individual QD's is much closer to that of the band gap than the luminescence arising from large ensembles of QD's from the same sample. In fact, the large ensemble behavior can be explained by the fast quenching of the smaller dot emission by the thermal escape of carriers to the barrier[1,5] or to the wetting layer.[2–4] Indeed, the quenching of the intensity with temperature is well described by activation energies of the order of the energy difference between the QD exciton ground states and either the barrier band gap[5] or the WL ground state.[2,3] Once in the barrier or the WL, the carriers are either lost through recombination or recaptured by the QD's. The radiative emission from larger QD's is thus favored over that from smaller ones when increasing the temperature. Furthermore, the quenching of smaller dot emission by thermal escape often results in weak emission intensity at room temperature (RT) for the InAs/GaAs system, as less than about 6% of the low-temperature emission remains for larger dots emitting in the 1–1.2 eV region,[4–6] and 0.1% for emission over 1.25 eV.[2,3,5] The same general temperature behavior has been observed for thin InAs/InP(001) QD's emitting at high energy, upward from 0.95 eV.[12]

In contrast, for larger InAs/InP QD's emitting in the 0.6–0.95 eV region for which the carriers are well confined, strong RT luminescence has been observed, typically of the order of 30%–50% of the LT intensity.[8,10,12–14] Bansal *et al.*[10] have in addition observed a different behavior from the various components of a multimodal emission: the low-energy (0.6 eV) peak intensity drops faster than that at 0.8 eV, while the high-energy contribution (1 eV) quenches much more rapidly than the other two. Also, the temperature-induced redshift of around 70 meV found by Chouaib *et al.*[15] for the emission peaks of InAs/InP(001) quantum sticks emitting in the 0.8–

0.95 eV region is consistent with the expected InAs bandgap shrinkage. The overall temperature dependence of the PL from InAs/InP QD's emitting below 0.95 eV is therefore quite different from that for the InAs/GaAs system, for which the carriers are much less confined.

For QD multilayers, a large carrier confinement should improve even more the temperature stability of the PL emission. Indeed, the deterioration of the barrier material quality when reducing the spacer layer thickness has been shown to have a major impact on the emission intensity as strain-induced nonradiative centers reduce the transfer efficiency of the carriers toward the QD's for InAs/GaAs (Ref. 16) and InAs/InAlGaAs on an InP substrate.[17] In addition, Sanguinetti *et al.*[16] have shown that for InAs/GaAs multilayers with thin spacers, the PL intensity drops faster with temperature when increasing the number of layers. Still, Mazur *et al.*[18] have shown that is it possible to improve the temperature stability of the optical properties in that material system by taking advantage of the coupling between vertically aligned pairs of QD's that favors emission from larger dots (with deeper confinement).

In summary, while the dynamics of the carriers between the QD's of different sizes, the WL, and the barriers is well understood in systems with rather weak confinement, the temperature-activated processes that deteriorate PL emission in systems with well-confined carriers, such as relatively thick InAs/InP QD's, remain unclear. In addition, the consequences of stacking vertically aligned islands on the stability of the optical properties as a function of temperature have yet to be explored.

We have therefore investigated the temperature dependence of the optical emission from multilayers comprising one to four planes of self-assembled InAs QD's in an InP matrix. The growth conditions were adjusted so as to obtain QD ensembles emitting in the 0.6–0.8 eV spectral region. We have found that the temperature-induced redshift of the emission in these heterostructures is smaller than that for the bulk InAs band gap. In addition, the PL intensity remains rather strong at room temperature, whereas the higher-energy contributions to the spectra increase with temperature. The stacking of aligned QD layers changes the carrier dynamics from the second deposited layer and up, and leads to an increase of the ratio between the QD and the WL signal intensities at low temperature. The results are explained using (i) temperature-dependent approximate effective-mass calculations to allow discrimination of the otherwise indiscernible contributions of the different QD families to the spectra, combined with (ii) a rate-equation model to explain the size-dependent carrier dynamics between the dots and the WL. Remarkably, no interlayer coupling was deemed necessary to quantitatively explain the PL observations for these closely spaced QD multilayers. Our experimental results can be explained by the quenching of the emission from the thicker dots at RT through thermalization of the carriers to excited nearly dark states and preferential transfer of the carriers initially captured by the WL to the thinner QD's, within the same layer.

II. EXPERIMENTAL DETAILS

The samples were grown on Fe-doped InP(001) oriented substrates by metalorganic vapor phase epitaxy in a cold-wall reactor.[19] We have used trimethylindium (TMIn), tertiarybutylarsine (TBAs), and tertiarybutylphosphine (TBP) as precursors, and Pd-purified hydrogen as the carrier gas. The reactor pressure was kept at 40 Torr and the precursor supply flow rates were 0.09 μmol s^{-1} for TMIn, 1.1 μmol s^{-1} for TBAs, and 4.2 μmol s^{-1} for TBP. After a 10-min annealing, of the substrate under TBP at 600 °C, a 140-nm-thick buffer layer was deposited with a susceptor temperature T_s of 600 °C. The buffer layer was then followed by an InAs/InP multilayer, where the InAs layers are grown in the SK mode, leading to QD's on a wetting layer [see Fig. 1(a) for a schematic representation of a bilayer structure]. Both the InAs and the InP spacing layers were grown at $T_s = 500$ °C. For each QD layer, the deposition of InAs (8 s) was followed by a 60 s growth interruption under a TBAs/H_2 ambient to promote island formation.[7] The gas interruption sequence required to obtain abrupt interfaces has been described in Ref. 7. The deposition of the last InAs layer of each sample was followed by the deposition of an InP precap of around 10 nm at 500 °C. The susceptor temperature was then raised to 600 °C to complete the deposition of the capping layer to a total thickness of ~30 nm. For thin spacer layers, QD's tend to be aligned on top of each other with increasing island size from one layer to the next.[20–22] We have grown multilayers up to four periods, varying the spacer thickness to bring the QD's of different layers as close as possible.

Photoluminescence measurements were carried out as a function of temperature in a He-flow cryostat using the 532 nm line of a solid-state laser as the excitation source within the linear excitation regime. The signal was acquired using a DA8 Bomem Fourier transform spectrometer with a nitrogen-cooled InSb detector.

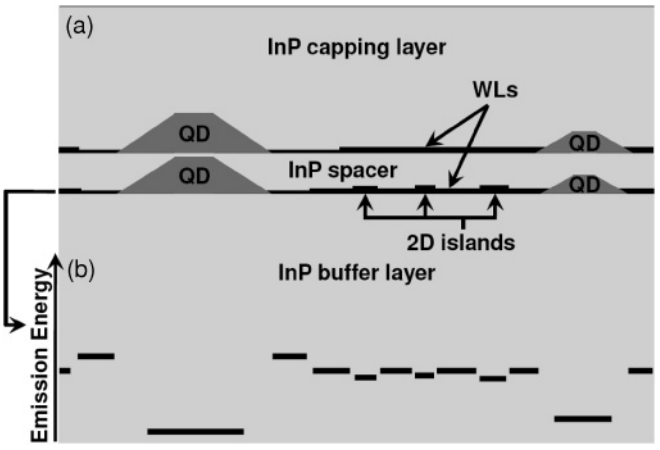

FIG. 1. (a) Schematic representation of the bilayer sample, showing a multilayer of InAs(P) 3D QD's (dark gray) formed on a WL (black) of the same material and embedded in an InP matrix. The modulation of the WL thickness generates some thicker 2D islands that confine the carriers laterally. (b) Simplified schematic illustration of the variation of the emission energy levels associated with the structures presented on the bottom InAs(P) layer.

Transmission electron microscopy (TEM) observations were made at 200 keV using a JEOL 2100F instrument. The scanning mode (STEM) images were acquired using a high-angular annular dark-field detector (HAADFD) to obtain a chemical contrast.

III. RESULTS

We can observe in Fig. 2(a), which presents a plan-view TEM micrograph of the single-layer sample, that the first layer deposited in these conditions has a planar density of 6×10^9 cm^{-2} fully coherent QD's, with diameters mostly comprised between 30 and 50 nm. With typical aspect ratios being of 0.1–0.2 for such nanostructures (from cross-sectional TEM observations of various samples in Ref. 22), we thus expect the nanostructure height to be in the 3–10 nm range.

Figure 2(b) shows an example of an aligned pair of QD's for the bilayer sample with nominal spacer layer thickness $H = 4.6$ nm. In contrast with the schematic representation of a bilayer presented in Fig. 1(a), we can observe that the spacer layer is not flat and that the separation distance between QD pairs is ∼2.5 nm. Trying to bring the QD's even closer, with $H = 3$ nm, we have observed that the growth of the second QD layer was inhibited in most areas. In the same way, for $H = 4.6$ nm, there are only two complete and distinguishable QD layers when nominally depositing four, and the PL spectra, at all temperatures, are very similar to the bilayer ones, but extend further in both low- and high-energy sides [the full width at half-maximum (FWHM) is a few tens of a milli-electronvolt larger]. Increasing the spacers to nominally 6 nm permits us to distinguish at least three layers of QD's, as shown in Fig. 2(c). Since it is hard to distinguish between the different structures of the upper layers, the spacers being too thin to flatten, it is not clear if the fourth layer is complete. Indeed, with cross-section images being projections of all structures contained in the TEM specimen (∼100 nm thick) along the [110] direction, there is a superposition of the contrast arising from the InP spacers and different InAs(P) layers, for the curvy upper layers. We can, however, observe that the alignment angle of the higher QD's is shifted from the growth direction and that the base of these dots is concave. As a result, the systematic height increase through closely stacked multilayers may be inhibited.

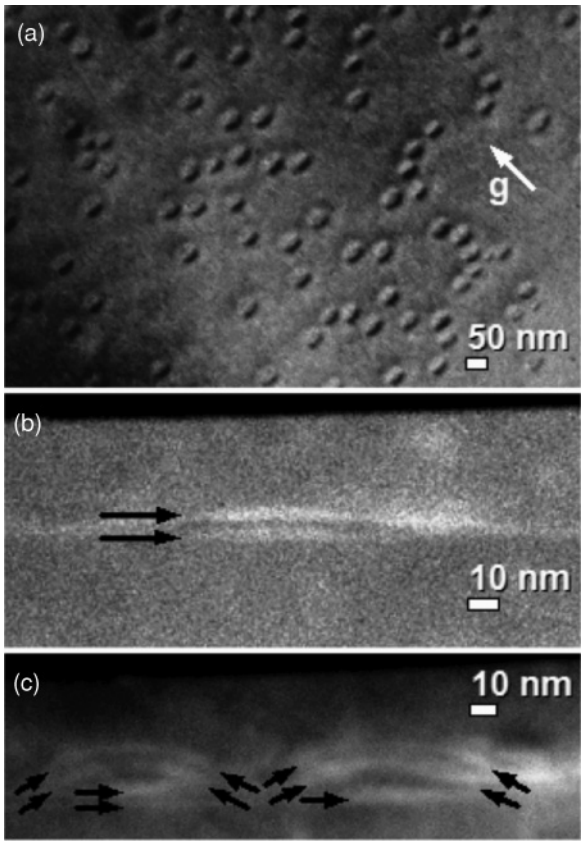

FIG. 2. (a) Plan-view TEM micrograph (bright field, $\mathbf{g} = 002$) of the single layer sample. (b) and (c) HAADF STEM images ([110] zone axis), with black arrows pointing toward the QD's, showing (b) an aligned pair of QD's from the bilayer with nominal spacer thickness $H = 4.6$ nm, and (c) columns of QD's from the four-layer sample, for which $H = 6$ nm. The superior layers being very curvy, the alignment of the upper QD's is shifted to an oblique angle with respect to the growth direction and their base is concave. Note that since TEM images are projections of the entire specimen thickness, the 3D deformation of the layers causes a superposition of the contrast originating from the spacers and different InAs(P) layers.

We present optical emission results from the three samples presented in Fig. 2 and nominally containing (a) a single InAs layer, (b) two InAs layers separated by 4.6 nm, and (c) the four-layer sample with 6 nm spacers. The PL spectra, acquired at temperatures ranging from 8 to 293 K, are presented in Fig. 3. The broad emission in the 0.6–0.8 eV range is attributed to the QD's, while the structures at much higher energies, near 1.15–1.25 eV, correspond to emission from the WL's. We will first compare the results obtained at low temperature for the three samples. We will then concentrate on the evolution of the PL spectra with temperature.

The QD emission band in the low-temperature (LT) spectra for the single-layer sample presents a maximum peak [labeled A in Fig. 3(a)] at 0.668 eV and a shoulder (B) at 0.723 eV. The uncertainty on the energy of the peak positions is less than 2 meV. Shoulder B most likely corresponds to emission from a group of smaller dots, rather than excited states, since measurements as a function of excitation intensity reveal that this feature remains present at much lower excitation power densities, with the same relative intensity (linear regime). The bilayer sample [Fig. 3(b)] presents two peaks of similar intensity at LT: peak C at 0.646 eV and D at 0.674 eV, with peak C arising essentially from the second deposited QD layer (the rest of the spectrum originates from the two layers). Indeed, the LT emission from the one-period sample is negligible at 0.646 eV; the presence of this lower-energy emission peak in the two-layer sample can be attributed to the fact that vertically aligned nano-islands tend to grow larger for subsequent layers.[20–22] The LT spectrum from the four-layer sample [Fig. 3(c)] presents a rather smooth peak at 0.680 eV with a FWHM of 65 meV. Even though its maximum is at an energy higher than peaks A and D, the LT spectrum from the four-layer sample extends comparatively further toward low energies. Emission from the three samples extends to about the same high-energy value and, surprisingly, the relative importance of the higher-energy contributions increases with the number of layers deposited, in spite of the fact that the spectra extend to lower energies.

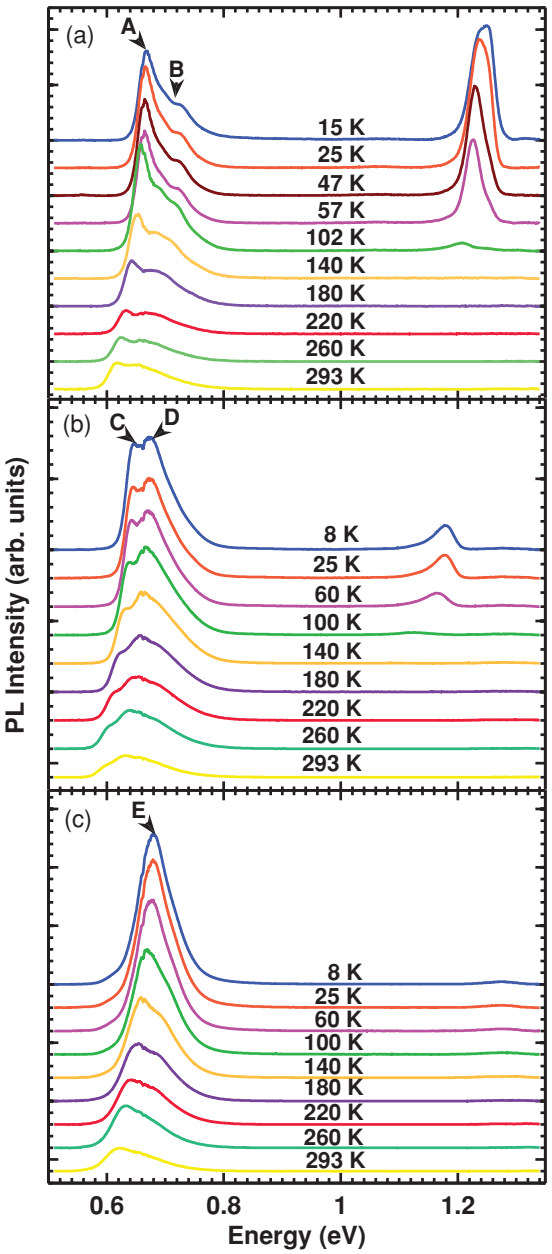

FIG. 3. (Color online) Temperature dependence of the photoluminescence spectra (shifted for visualization) for samples with (a) one, (b) two, and (c) four QD layers. The arrows indicate the characteristic peaks followed in Fig. 5.

One can observe that the LT emission from the WL's decreases rapidly with an increasing number of QD periods. Indeed, the integrated PL intensity data in Fig. 4(a) reveal that the LT emission from the WL of the single-layer sample is nearly equal to that from the QD's: it represents 49% of the total integrated intensity. This proportion drops to 11% and becomes negligible when depositing two and four layers, respectively. Also, comparing Figs. 3(a) and 3(b), we note that the WL signal for the bilayer sample is shifted to lower energies than that from the single-layer sample. Although our PL measurement setup does not allow for a precise comparison of the absolute values of the emission intensities (uncertainty of 25%) between different samples, Fig. 4 reveals that the

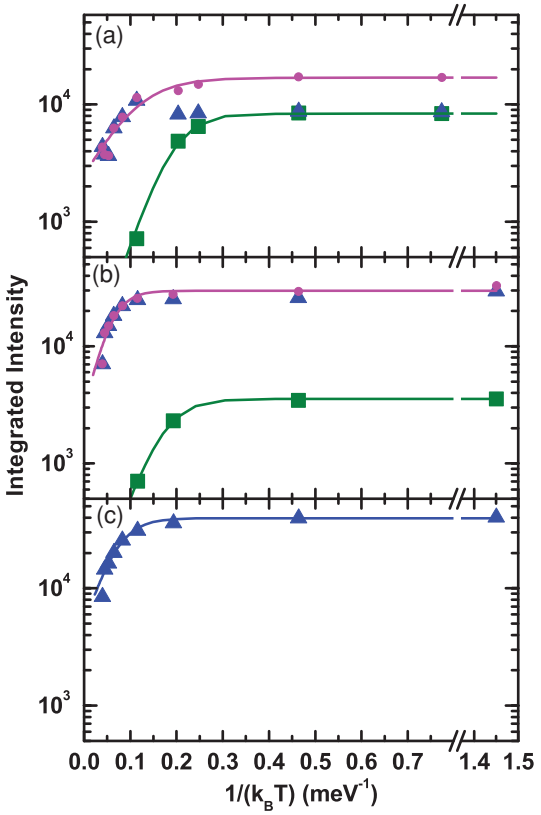

FIG. 4. (Color online) Temperature dependence of the PL integrated intensity from QD's (triangles) and WL (squares) for the (a) one-, (b) two-, and (c) four-layer samples. The circles in (a) and (b) represent the total intensity, i.e., the sum of the QD and WL signals. The solid lines correspond to fits of Eq. (1) to the data with parameters presented in Table I.

integrated emission intensity from the bilayer sample is about twice that for the single layer one. The total intensity from the four-layer sample is, however, only a factor of 2.4 ± 0.6 larger than that of the single-layer. We attribute this result to the fact that excessive strain in the deformed upper spacer layers results in a large defect density, as was previously suggested for InAs/GaAs (Ref. 16) and InAs/InAlGaAs on InP substrate[17] multilayers with thin spacer layers. Yet the intensity of the QD emission bands varies superlinearly with the number of layers, being 3 and 4.5 times the single-layer (SL) one for the bilayer (BL) and the four-layer sample, respectively.

Increasing the PL measurement temperature leads to an almost complete quenching of the WL emission by 100 K, whereas the integrated intensity from the QD's decreases much more slowly: the RT integrated intensities of the PL emission from the QD's are 51%, 24%, and 21% of their LT value for the one-, two-, and four-period samples, respectively. Figures 3(a) and 4(a) clearly show that emission from the QD's increases near 100 K for the single-layer sample, therefore indicating that the WL signal is not lost through nonradiative recombination when increasing temperature up to 100 K, but rather transferred from the WL to the QD's. The higher room- to low-temperature intensity ratio obtained for the dot emission from the single-layer sample is thus a consequence of this large number of additional carriers, transferring from the WL for temperatures

higher than 100 K. Comparing instead the evolution of the total emission (combined from both the WL's and the QD's) with temperature for the three samples, we obtain that the RT emission corresponds to 26% of the total LT intensity for this sample, close to the value of 21% obtained for both multilayer samples.

As the temperature is raised from around 100 K and up, one can observe in Fig. 3 that the relative intensities of the higher-energy contributions to the QD bands (corresponding to emission from either the thinner dots in the samples or to excited states) increase in agreement with what was found by Bansal *et al.*[10] for the same material system. Also, the RT spectra are broad and rather flat, in particular the one from the single layer. Results from Fig. 3 are replotted in Fig. 5 as *normalized* PL intensity data from QD's as a function of the energy for each temperature at which a spectrum has been taken. The color scale [located above Fig 5(a)] is the same for the three graphs, with half-maximum values corresponding to green. We can see that for the three samples, the FWHM of the QD emission increases monotonically with temperature up to around 220 K and then stabilizes up to RT to a value around 100 meV. The low-temperature FWHM values, however, differ more significantly from one sample to the other. The FWHM of the signal from the single layer at LT is half that at room temperature, and its value increases rapidly between 60 and 140 K as the WL signal is quenched. The two- and four-layer bandwidths are larger at LT, being 78% and 67%, respectively, of the FWHM at 293 K.

To study the temperature dependence of the QD emission energy, we have followed peaks A to E in Fig. 3. The data, corresponding to maxima of intensity (no deconvolution), are presented in Fig. 5 as circle and triangular markers. For peaks A, C, and D, we observe a redshift of 46, 44, and 41 meV, respectively, between low and room temperature. The maximum of the four-layer signal (E), however, shifts by 58 meV, which is close to the 63 meV value predicted for bulk InAs by Varshni's law using the generally accepted parameters[23] found by Fang *et al.*[24] (the shift between 0 and 15 K is negligible, the theoretical value being 0.6 meV). Shoulder B, in the single-layer spectra, redshifts by 20 meV between 8 and 140 K (it cannot be clearly resolved above the latter temperature), the same value as for the four-layer sample maximum (E), and close to the 24 meV value predicted by Varshni's law for the variation of the bulk InAs band gap. In contrast, the redshift at 140 K is significantly smaller for peaks A (15 meV), C (14 meV), and D (12 meV).

Further observations of the WL signals in Figs. 3(a) and 3(b) reveal that their peak maxima redshift much faster than those for the QD's. The rapid quenching of the high-energy components of the WL spectra is accompanied by a significant intensity transfer to lower-energy features and a decrease of the WL emission bandwidth, in contrast with the emission from QD's.

IV. DISCUSSION

A. Carrier transfers between QD's and WL's

The LT emission bands from the WL's are fairly wide, reflecting the roughness of the WL's that, according to the

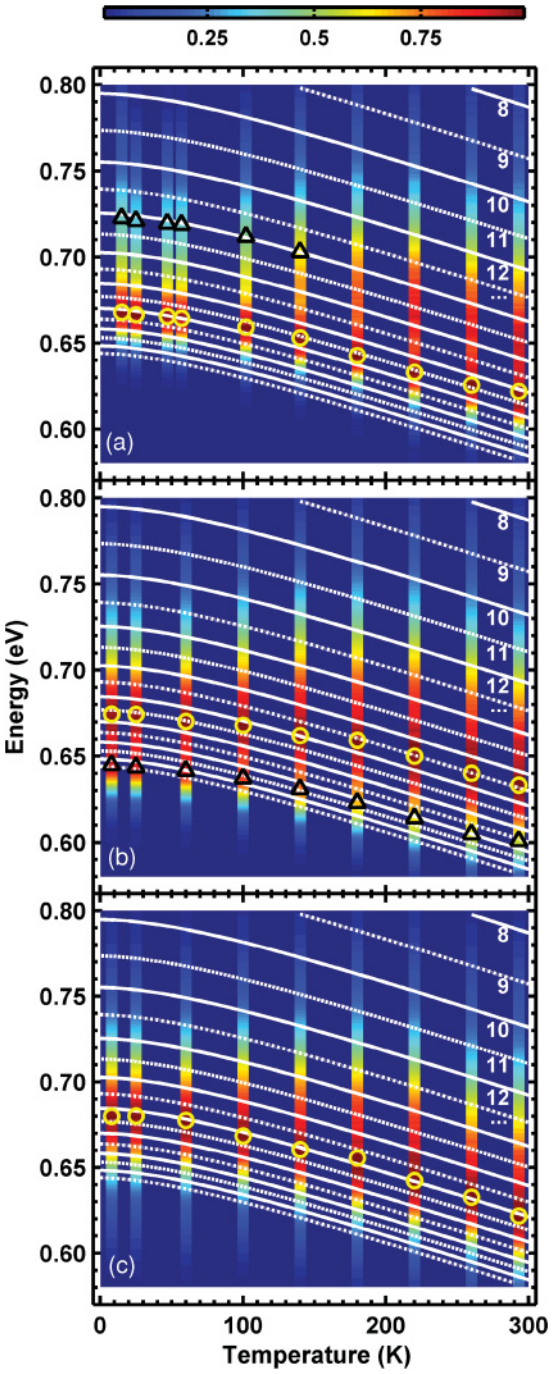

FIG. 5. (Color online) Energy of the characteristic peaks labeled in Fig. 3 as a function of temperature: (a) Maximum peak A (circles) and shoulder B (triangles) from the spectra of the single-layer sample, (b) peaks D (circles) and C (triangles) from the bilayer sample, and (c) maximum peak E from the four-layer sample spectra. The color stripes correspond to the normalized PL intensity data as a function of energy (see color scale above) for each temperature at which a spectrum has been measured. The increase of the full width at half maximum with temperature for the QD emission can be visually followed. The white curves represent the calculated results for $InAs_{0.905}P_{0.095}$ quantum-well layers of an integer number of ML's (indicated below the line for the first five ones). Solid and dotted lines alternate for clarity of presentation.

spectra, may contain thin (2–3 ML) 2D islands with a large distribution of lateral size, as schematically shown in Fig. 1(a). Those 2D islands are formed by the modulation of the flat WL thickness, in contrast with 3D islands grown in the SK mode (to which we refer when we use the term "quantum dots"). The thicker 2D islands (3 ML) can effectively confine the charge carriers [Fig. 1(b)] and reduce their transfer toward the QD's. We interpret the rapid shift of the peak maxima as a consequence of the thermal escape of the carriers out of the 2D islands of smaller lateral size of the WL's, where the confinement is weaker, and a further transfer to the more favorable radiative recombination sites, either the QD's or the larger 2D islands, for which the ground-state energy is lower.

Further information can be obtained by determining the activation energy of the PL intensity quenching, by means of a least-squares fit of the temperature dependence of the PL integrated intensity (I_{PL}) for the data sets presented in Fig. 4 to the following function:[1,2,25,26]

$$I_{PL} = \frac{I_0}{1 + C\ \exp(-E_a/k_B T)}, \tag{1}$$

where I_0 is the intensity at low temperature, the prefactor C is a dimensionless constant, and E_a is an activation energy. Equation (1) is not appropriate to fit the QD emission integrated intensity for the one- and two-layer samples on the whole temperature range because of the additional intensity transferred from the WL around 100 K. In addition, from this temperature up, the radiative emission originates quasi-uniquely from the QD's (see Fig. 3), such that these data points are superposed to that for the total intensity. Therefore, we have fitted only the integrated intensity data corresponding to the signal from the WL and the total emission with Eq. (1). The QD intensities will be treated using a more suitable equation set, obtained from a rate-equation model in Sec. IV C. The values of E_a (with 95% confidence interval) and C giving the best fits to Eq. (1) (solid lines in Fig. 4) are presented in Table I. The confidence intervals given for C (in brackets in Table I) are delimited by the values minimizing the least-mean-square residue for the two E_a confidence boundaries. For all data sets, the activation energy obtained for the average behavior of the emission bands is of the order of a few tens of meV. For the WL's, this is consistent with our hypothesis that the activated process leading to the quenching of their signal is the escape of the carriers out of the 2D islands, based on calculations by Shtinkov *et al.*[27] for such nanostructures formed by the thickness modulation (2–3 ML) of a thin InAs layer deposited on an InP substrate.

TABLE I. Parameters used to fit Eq. (1) to the data of Fig. 4 for the integrated intensity emitted from the wetting layer (WL) and for the total emission integrated intensity (Total). The values of E_a are given with a 95% confidence interval. The confidence intervals (in brackets) for C are delimited by the values minimizing the least-mean-square residue for the two E_a confidence boundaries.

	E_a (meV)		C	
Number of periods	WL	Total	WL	Total
1	27 ± 7	18 ± 7	176 [47, 814]	6 [3, 10]
2	26 ± 9	39 ± 19	83 [19, 396]	9 [3, 25]
4		30 ± 10		7 [4, 14]

However, the value obtained from the total spectrum is not necessarily quantitatively significant, since the activation energy is expected to depend on the dot size. Still, our results confirm that the thermal escape of the carriers toward the barriers (or to the WL's, for the QD's) is not an important path to nonradiative recombination, even for the carriers that are weakly confined in the WL's, since if that were the case we would have obtained activation energies of a few hundreds of meV.

Besides, we have seen that the emission from the QD's is clearly favored at LT for multilayers. Close stacking of dot layers thus affects the carrier dynamics between QD's and WL's. For example, the integrated intensity of the emission from the QD's of the bilayer $(I_{QD0})^{BL}$ at low temperature is thrice that of the single-layer sample $(I_{QD0})^{SL}$. Since the intensity arising from the QD's of the first (bottom) of the two layers should be at most equal to that from the SL sample, the emission from the second layer of the BL is thus $(i_{QD0})_2^{BL} \approx 2(I_{QD0})^{SL} \approx (I_{QD0})^{SL} + (I_{WL0})^{SL}$. Therefore, nearly all photogenerated carriers captured by the second WL are directly transferred to the QD's even at low temperature, so I_{WL} comes mainly from the first deposited one. This is probably due to the fact that the WL's (from the second one and up) are thinner in stacks of vertically aligned dots,[28] and are consequently likely to contain fewer 3-ML-thick 2D islands that can effectively trap the carriers in the wetting layers.

On the other hand, despite the close stacking of the QD layers, our results show no evidence of an electronic coupling between nanostructures from different layers. Such a coupling should favor emission from lower-energy states. Yet we have obtained an increase of the intensity from higher-energy states with the number of layers, even for much lower power density (the PL measurement are executed in the linear regime). In fact, since the penetration of the carrier wave function decreases exponentially with the energy barrier height (confinement of the carrier), the QD's must be placed much closer in multilayers of thick InAs/InP in comparison with systems for which the carriers are less deeply confined, such as InAs/GaAs. As a consequence, it is likely that the separation distances of a few nanometers between the InAs layers in our samples are still too large to obtain an observable interaction between the dots.

B. Size dependence of the temperature behavior of the QD luminescence

To analyze the size-dependent temperature behavior, we assume that the emission energies for these laterally extended QD's can be obtained by separating them in families whose spectra are primarily determined by the QD height. Indeed, since the lateral confinement energy in these low-aspect-ratio InAs/InP QD structures is small,[7] we can reasonably describe their emission energies using those for quantum wells (QW's) with the same number of monolayers (ML's).[9,11,29] The excited states due to the lateral confinement, since they lie only a few meV above the ground state, should cause a widening of the emission peaks of each family (associated with a ground state and eventually excited states arising from vertical

confinement), as does the lateral size distribution of dots of the same height, in addition to a slight blueshift.

Calculations of the emission energy can take into account the effect of temperature on the material band gap and on the strain, and therefore on the confined energy levels of the charge carriers. To do so, we have calculated the fundamental electron–heavy-hole transition ($e1$-hh1) for $InAs_{1-x}P_x$/InP QW's using the envelope-function approximation (EFA) for finite rectangular wells. The effect of biaxial strain $\varepsilon_{||}$ has been taken into account using the Pikus and Bir Hamiltonian:[30] the gap is increased by $2a_H(1 - c_{12}/c_{11})\varepsilon_{||} - b(1 + 2c_{12}/c_{11})\varepsilon_{||}$. The coefficients a_H and b are the hydrostatic and shear deformation potential of the alloy. This calculation reproduces fairly well the results for the $e1$-hh1 transition calculated with other EFA-based techniques, i.e., with the eight-band **k**.**P** theory[9] and the Bastard-Marzin Hamiltonian[31] at 0 K. We have neglected the exciton binding energy, which should be less than 10 meV for our type of structures.[31,32] Following Zhao *et al.*,[33] we have assumed that the elastic constants c_{11} and c_{12} vary with T as described in Refs. 34 and 35, and that a_H, b, and the hole effective masses are independent of temperature. For the electron effective masses, we have used the approximation derived from **k**.**P** theory, as suggested by Vurgaftman *et al.*[23] The biaxial strain $\varepsilon_{||}$ has been calculated using the values of Ref. 36 for the temperature-dependent relaxed lattice parameters of the substrate and the layer. We have used an unstrained valence-band offset (VBO) value of 0.35 eV between InAs and InP at 0 K.[23] Based on the results of Ref. 31, the resulting fraction of the strained electron well depth on the total strained band-gap difference $\delta E_c \equiv \Delta E_e^{\mathrm{str}}/\Delta E_g^{\mathrm{str}} = 0.51$ was kept constant when varying the temperature or QW composition x. For the dependence in x, a linear interpolation of the unstrained VBO would have given a result very close to keeping δE_c constant. For all other parameters, we have made a linear interpolation between InAs and InP values when varying composition, except for the band gap and the spin-orbit splitting, for which we have added bowing parameters $c = 0.1$ and 0.16, respectively.[23] For the temperature dependence of the band gaps, we have used the Varshni coefficients of Fang *et al.*[24] for InAs and the Bose-Einstein-type dependence found by Hang *et al.*[37] for InP. The latter, combined with the accepted InAs band-gap dependence, gives an excellent fit to the results obtained by Zhao *et al.*[33] for the temperature dependence of $InAs_{1-x}P_x$ (high x) QW's, much better than that obtained when using the Varshni relation with the coefficients proposed in Ref. 23 for the InP band gap.

For $\delta E_c = 0.51 \pm 0.03$ (VBO between 0.3 and 0.4 eV), we obtain agreement between the calculations and the experimental luminescence signal corresponding to a WL thickness of 2–3 ML for a composition x comprised between 8% and 12%, assuming the same composition throughout the multilayers. This results in an indexing of the LT spectrum from the single-layer QDs varying between 11 and 21 ML (3–7 nm) for 8% and 13–31 ML (4–10 nm) for 12%. This is coherent with the distribution of diameters observed in the TEM plane view. Intermixing between As and P is expected to occur during the growth of such samples; the composition that we have deduced agrees well with those found for much thinner InAs layers deposited with the same system ($x = 12\%$ using **k**.**P** theory)[9] and for QD's grown by chemical beam epitaxy ($x = 6\%$–10% based on tight-binding calculations).[11]

The white curves in Fig. 5 correspond to the results of our calculation for $InAs_{0.905}P_{0.095}$ QW's with 8–25 ML, corresponding to QD families of the same height labeled as $f8$ to $f25$. The total redshifts (from LT to RT) calculated for those families are slightly smaller than that for the bulk material, but not nearly enough to explain the behavior of peaks A, C, and D. One can see, however, that peaks B and E follow well the temperature dependence of $f14$ and $f18$, respectively. Low-temperature peaks A, C, and D can be associated with $f20$, $f24$ (at 60 K), and $f19$, respectively. When increasing the temperature, emission peak A shifts from $f20$ to $f19$ between 57 and 140 K. It then follows the temperature dependence of $f19$ to about 260 K, and finally shifts again to follow an energy corresponding to a QW of 18 ML at RT. The intensity at RT is, however, practically flat between $f15$ and $f19$. Peaks C and D also shift down a family between 60 and 140 K, and yet again at 180 K, at which temperature their emission corresponds, respectively, to 22- and 17-ML-thick QW's. They follow those families up to 260 K. Finally, at RT, peaks C and D are, respectively, centered on energies corresponding to $f21$ and $f17$, but the maximum intensity is actually distributed between $f15$ and $f18$, in contrast with the LT spectrum, for which the highest intensity corresponds to $f18$–25.

The increased filling with temperature of the excited states due to lateral confinement could contribute to the reduced redshift of the peaks of lower energy, A, C, and D. Still, this minor effect does not explain the general behavior of our sample luminescence, which is the relative increase of the higher-energy contributions to the QD spectra with temperature. Indeed, measuring the FWHM of the spectra in terms of its corresponding families, we find, from LT to RT, (a) $f16$–23 to $f11$–21 for the single layer; (b) $f15$–29 to $f11$–22 for the bilayer; and (c) $f15$–23 to $f12$–22 for the four-layer sample. This is due, in addition to the relative rise of the intensity at energies corresponding to thinner families when increasing temperature, to a relative loss of the emission intensity from the thicker (lower-energy) QD families as compared to the maximum peak, in particular for the bilayer sample. Indeed, the FWHM of the bilayer spectrum at LT extends quite further toward low energies than that of the other two samples, while the spectral range at half-maximum of the PL is practically the same for the three samples at 293 K.

To visualize the size-dependent temperature behavior of the QD luminescence more easily, we present in Fig. 6 the experimental value of the absolute emission intensity at the $e1$-hh1 energy calculated (including the temperature-induced redshift) for each family. First, one can observe that the intensity drop caused by the loss of carriers through nonradiative channels occurs at lower temperature for the thicker dots. Second, the absolute intensity at energies corresponding to thinner QD's actually increases slowly with temperature (up to about 100 K for the single layer and 140 K for the multilayers), as shown in Fig. 6. The latter effect is barely observable for the four-period multilayer.

Those high-energy contributions to the QD signal may originate from thin family ground states and/or thicker dot excited states. An explanation of the emission broadening

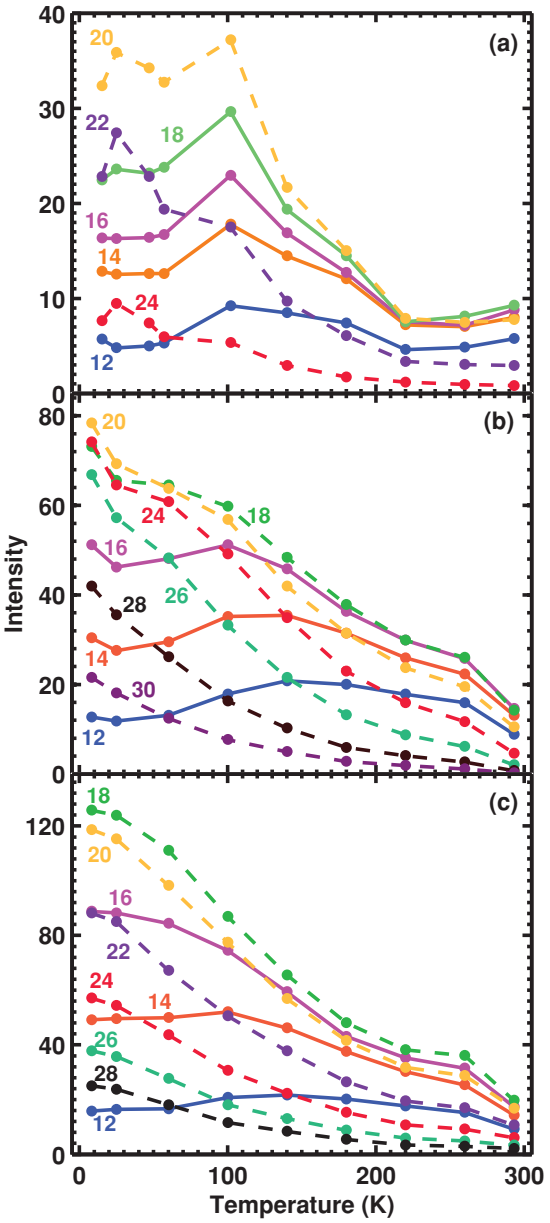

FIG. 6. (Color online) Absolute experimental emission intensity from a specified QD family as a function of temperature, considering the redshifts calculated for an $InAs_{0.905}P_{0.095}$ quantum well of the same thickness (white curves in Fig. 5). The family index is given next to each curve. The lines (dotted for families of index equal to or higher than that of the family of maximum intensity at low temperature) are a guide for the eyes.

with increasing temperature (in place of the apparent transfer to higher-energy families) could simply be the population of excited states (excited states due to vertical confinement, as will be understood to be the case from now on). Carrier intraband transitions can, in principle, populate excited states such as the second electron confined level ($e2$), the second confined heavy-hole level (hh2), or the first confined light-hole levels (lh1). Our calculations reveal that, for wells thicker than 7 ML, the hh2 states are the closest in energy to the ground states. However, it is very unlikely that they participate in the radiative emission through the $e1$-hh2 transition, because the latter is forbidden for QW's and therefore should be weak in the case of QD's with small lateral confinement. The closest allowed interband transition for QW's is $e1$-lh1. Since our calculations indicate that those states lie at least 165 meV over the ground state for $f10$–35, which is larger than the bandwidth of the spectra, the population of these states is also unlikely to explain our results.

In addition, it should be emphasized that there is a strong correlation between the intensity rise of high-energy QD states and the quenching of the WL signals. First, they occur in the same temperature range, i.e., between 50 and 140 K. Second, the intensity increase becomes less important with the number of InAs(P) layers and is in fact proportional to the LT intensity of the WL signal. Note that the fact that this additional source of carriers as the temperature increases favors emission at higher energies is not due to saturation of lower-energy states, since we are in the linear excitation regime. This suggests that the temperature behavior of the luminescence is more probably due to a dot-size dependence of the carrier transfers from the WL, rather than to radiative recombination from excited states.

We thus interpret the rise of the absolute intensity of the emission from high-energy QD states in the following way: the carriers initially captured by the WL are transferred only toward the thinner QD families. This can be explained using the results of Landin *et al.*,[8] who have observed a 110 meV activation energy for the quenching of the PL from the WL following the transfer of the carriers to the QD's. They have attributed this behavior to the thinning from 2 to 1 ML of the surrounding WL during the ripening of larger 3D islands grown in the SK mode, which was previously observed.[38] Such thinning would induce an energy barrier for the carriers to overcome when transferring from the WL to the larger QD's. The experimental activation energy value that they have obtained is consistent with our calculations, which indicate a value of 117 meV for such an energy barrier (for the excitons). Shoulder B of the single-layer sample is in fact probably due to the fact that emissions from thinner dots are favored: the WL is an additional source of carriers for the corresponding dots.

Moreover, this interpretation, combined with the observation mentioned earlier that the second and subsequent WL's transfer more carriers toward QD's than the first deposited one, can explain the effect of the number of layers on the extent of the spectra, for thin-spacer multilayers. One can observe from the data in Fig. 6 the relative increase of each family's intensity with the number of layers deposited. Obviously, the maximum increase occurs for large QD's of height over 23 ML, because of the increase of the QD average height in these thin-spacer multilayers. However, intensities corresponding to $f15$–18, which can be fed by the WL's in the frame of our hypothesis, increase more (over three and five times the SL values for the BL and the four-layer samples, respectively) than those associated with $f19$–22. Moreover, the hypothesis that nearly all of the carriers initially captured by the second, third, and fourth wetting layers are transferred to thin QD's at low temperature is consistent with the fact that the maximum emission peak at LT for the four-layer sample occurs at higher energy in comparison with the other two. Thus, this interpretation leads to the conclusion that the PL spectra do not reflect the real size distribution of the SK 3D islands, since

the population of the smaller dots by carriers should be favored by transfers from the wetting layer. Our results show that this effect is accentuated by the increase of the temperature or of the number of layers deposited.

It should be noted that the curves presented in Fig. 6 are only indicative of the general behavior of the PL and are not intended to represent the exact intensity emitted from each of the families, due to the overlap of the different contributions to the spectra (the FWHM of each family is estimated to be of the order of a few tens of meV). In particular, the energy separation between two successive families decreases as the index increases, so the relative importance of the emission from thicker dots is overestimated in comparison with that from thinner ones. Since the emission peaks from each family are not distinguishable, a deconvolution of the spectra in our case would have been quite arbitrary and would not have led to more meaningful results than what we present in Fig. 6. Also, the exact indexing of the spectral features depends on the chosen material parameters, particularly on the composition. Indeed, the 2% uncertainty on the composition alone leads to a maximal uncertainty of ± 2 ML on the indexing of signals of energy $\geqslant 0.7$ eV, but it increases rapidly for lower energies, again due to the decrease of family separation with the increase of nanostructure thickness. A change of the unstrained VBO of ± 50 meV, however, has a negligible influence on the calculated energies of the $e1$-hh1 transition for QW's $\geqslant$ 10 ML. Nevertheless, these uncertainties have no incidence on the conclusions drawn so far, i.e., that the nonradiative recombination of the carriers occurs at a lower temperature for thicker QD's and that the carrier transfer from the WL favors emission at energies corresponding to thinner dots.

C. Rate-equation model to describe the dot-size-dependent carrier dynamics

We have presented two possible explanations for the redistribution of the excitonic emission toward higher energies as the temperature increases: (a) the thermal occupation of the nearest excited state, hh2, and the subsequent $e1$-hh2 radiative recombination (which is forbidden in the QW case) or (b) the charge carriers initially captured by the WL are more efficiently transferred to the thinner QD's, which causes an increase of the intensity emitted from the thinner nanostructures as the carriers escape from the thin 2D islands of the WL.

The thermalization of the holes to the excited-state hh2 is consistent with the fact that the intensity quenches at lower temperature for larger dots: the hh1-hh2 energy separation decreases with increasing dot thickness. However, as already mentioned, the rise of high-energy contributions to the QD band occurs in the same temperature range as the quenching of the WL emission, independently of dot size. The most reasonable explanation for our experimental results thus seems to be the thermalization of the holes to excited nearly dark states (from which the probability of radiative recombination with electrons in their ground state is weak), combined with the preferential transfer of the carriers from the WL to the thinner QD's, which we will refer to as hypothesis (b). To demonstrate this, we have developed the simplest rate-equation model—describing the interaction between the QD's, the WL's, and the barriers, and the thermalization of carriers to excited states—that can reproduce our experimental results. The same model allows us to test hypothesis (a) as well, for which the radiative transition $e1$-hh2 would be the primary cause of additional high-energy emission to the QD spectra at high temperature.

Those two possibilities are presented schematically in Fig. 7 (see the caption for a detailed description), the difference between the two cases being only that, in the frame of hypothesis (b), we neglect the t_{3i} coefficients for thick QD's as well as the radiative recombination rate R_{Ei} for all subsets. We have grouped the QD states into subsets corresponding to our previously introduced families of nanostructures of the same height, where the QD energy levels are approximated by the ones calculated for QW's of the same thickness. Thus, subset Q_1 in Fig. 7 corresponds to the thinnest family considered, which is $f12$ in our calculation. The incident power density P is absorbed by the InP barrier layers (B) and the generated carriers can then transfer to the WL (W)

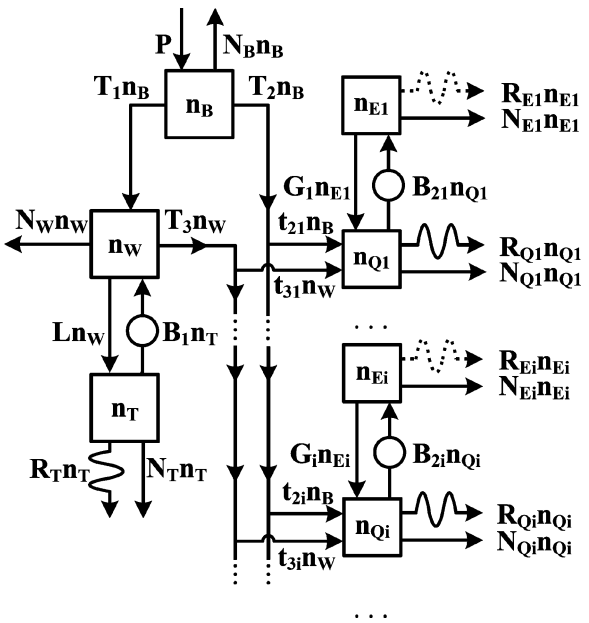

FIG. 7. Carrier transfer scheme proposed for the InAs/InP QD system and corresponding to the rate-equation model of Eqs. (2)–(5). The incident optical power density is represented by P. The alphabetic *indices* correspond to the following elements of the heterostructures, which are populated with a density n_x of carrier pairs (or excitons): the InP barriers (B), the WL (W), the traps (2D islands) that confine carriers in the WL (T), the fundamental levels of a subset i of QD's of the same height (Q_i), and their nearest excited state (E_i). The radiative and the nonradiative recombination rates are represented, respectively, by the R_x and N_x coefficients. The transfer coefficients T_n are T_1 between the barriers and the WL, $T_2 = \sum_i t_{2i}$ between the barriers and the QD's (transfer rates being different for each subset i), and $T_3 = \sum_i t_{3i}$ between the WL and the QD's. The trapping rate of the carriers in the WL is L and their rate of escape, which includes an energy barrier, is $B_1 = \Gamma_1 \exp(-E_{a1}/k_B T)$. For the QD's, the rate for the excitation to the nearest energy level is $B_{2i} = \Gamma_{2i} \exp(-E_{a2i}/k_B T)$, where E_{a2i} corresponds to the energy separation between the ground and excited states, while the relaxation to the ground level occurs at a rate G_i.

and the QD fundamental states (Q_i), or be lost through nonradiative recombination in the barriers. From the WL, the carriers can either be trapped in the thin 2D islands (T) due to layer roughness, be captured by the QD's, or be lost through nonradiative recombination. The emission from the WL is assumed to originate principally from the 3-ML-thick 2D islands, so we have neglected in our model the radiative recombination from the flat 2 ML layer (W) for the sake of simplicity. From the QD's, the carriers either recombine (radiative and nonradiative recombination) or the holes are excited to the hh2 levels (E_i). Transition rates including an energy barrier are given by $B_1 = \Gamma_1 \exp(-E_{a1}/kT)$ and $B_{2i} = \Gamma_{2i} \exp(-E_{2ai}/kT)$. For B_1, E_{a1} represents the energy barrier to escape from the WL 2D islands, and $E_{a2i} = \Delta\text{hh}_i$ is the energy separation between the fundamental and closest excited state for group i of QD's of the same height.

Thermal escape of the carriers from the QD's to the WL or to the barriers often is a strongly thermally activated process in less deeply confined QD systems.[1–5,12] They are, however, ignored in our simplified model, since the very large activation energies for thermal escapes into the WL or the InP barriers render these rates negligible for all practical purposes. Similarly, we have shown earlier that even for the less confined carriers in the WL, their efficient transfer toward the QD's disables their escape to the barrier, such that we can also neglect this process. In addition, since our PL results show no evidence of electronic coupling between QD's of different layers, we have not considered this phenomenon in the model.

Considering stationary states ($dn_x/dt = 0$), one obtains emission intensities I_x for an isolated layer given by Eqs. (2)–(4) below, depending on the hypothesis to be used. For the WL,

$$I_W = R_T n_T = \frac{\frac{PT_1L}{(T_1+T_2+N_B)(1+N_T/R_T)(T_3+L+N_W)}}{1+\frac{T_3+N_W}{T_3+L+N_W}\frac{\Gamma_1}{R_T+N_T}\exp(-E_{a1}/k_BT)} \equiv \frac{i_{W0}}{1+c_W\exp(-E_{a1}/k_BT)}, \quad (2)$$

with $i_{W0} = I_W(T=0)$. We therefore obtain Eq. (1), which fits well the WL intensity temperature dependence for both single-layer and bilayer samples, with parameters given in Table I.

For the ith QD subset, assuming that the radiative recombination $e1$-hh2 is efficient [hypothesis (a) above], i.e., $R_{Ei} \neq 0$, leads to

$$\begin{aligned} i_{Qi}^{(a)} &= R_{Qi}n_{Qi} + R_{Ei}n_{Ei} \\ &= \frac{\frac{Pt_{2i}}{(T_1+T_2+N_B)(1+N_{Qi}/R_{Qi})}}{1+\frac{R_{Ei}+N_{Ei}}{R_{Ei}+G_i+N_{Ei}}\frac{\Gamma_{2i}}{R_{Qi}+N_{Qi}}\exp(-\Delta\text{hh}_i/k_BT)} \\ &\quad\times\left[1+\frac{\frac{T_1t_{3i}}{t_{2i}(T_3+L+N_W)}\left[1+\frac{\Gamma_1}{R_T+N_T}\exp(-E_{a1}/k_BT)\right]}{1+\frac{T_3+N_W}{T_3+L+N_W}\frac{\Gamma_1}{R_T+N_T}\exp(-E_{a1}/k_BT)}\right] \\ &\quad\times\left[1+\frac{R_{Ei}}{R_{Ei}+G_i+N_{Ei}}\frac{\Gamma_{2i}}{R_{Qi}}\exp(-\Delta\text{hh}_i/k_BT)\right] \\ &\equiv \frac{\frac{i_{Q0i}}{1+A_i}}{1+c'_{Qi}\exp(-\Delta\text{hh}_i/k_BT)} \\ &\quad\times\left[1+A_i\frac{1+D\exp(-E_{a1}/k_BT)}{1+c_W\exp(-E_{a1}/k_BT)}\right] \\ &\quad\times[1+c_{Ei}\exp(-\Delta\text{hh}_i/k_BT)], \end{aligned} \quad (3)$$

with the total intensity for the QD's $i_{\text{QD}} = \sum_i i_{Qi}$ for a single layer, $T_2 = \sum_i t_{2i}$, $T_3 = \sum_i t_{3i}$, and $i_{Q0i} = i_{Qi}(T=0)$. The emission from the first term ($R_{Qi}n_{Qi}$) occurs at $E_i^{\text{GS}} = e1_i$-hh1_i, and that from the second term ($R_{Ei}n_{Ei}$) corresponds to the transition to higher-energy levels ($e1_i$-hh2_i), i.e., $E_i^{\text{ES}} = E_i^{\text{GS}} + \Delta\text{hh}_i$.

The exponential containing the activation energy Δhh_i appearing in the denominator, with calculated values of Δhh_i (for $x = 0.095$) varying from 24 meV for $f30$ to 110 meV for $f12$, fits well the intensity drop as a function of temperature for all the families. The same exponential appears at the numerator of the excited-state term in Eq. (3). It represents the increase with temperature of the higher-energy contributions to the spectra due to the radiative recombination involving excited states. However, the increases in intensity occur all at the same temperature and are well described by a single $\exp(-E_{a1}/k_BT)$ term (using the value of E_{a1} given in Table I), which leads to $c_{Ei} = R_{Ei} = 0$ values for all curves. In addition, plotting the intensity at energies E_i^{ES} as a function of the intensity of the corresponding ground states (at E_i^{GS}) for each temperature shows no correlation between them (not shown). It is therefore safe to conclude that the $e1$-hh2 transition is weak in our nanostructures, probably because lateral confinement is very small. This, again, supports our approach, in which QD's are modeled by QW heterostructures.

Having eliminated hypothesis (a), we now neglect the $e1$-hh2 radiative recombination with the holes in their excited state (i.e., we take $R_{Ei} = 0$). The excitation of the holes to the hh2 levels provides, however, a good description of the large QD temperature behavior. We can thus conclude that the thermalization of holes to their first excited level, followed by a nonradiative recombination process, is the main path for the temperature-activated loss of the QD luminescence.

The rates of transfer from the WL to the QD's (t_{3i}) would normally be presented without an energy barrier, as it seems to occur for the smaller QD's. They, however, strongly depend on the dot size within the frame of hypothesis (b): the carriers are not transferred from the WL to the larger QD's, probably due to the energy barrier of ~100 meV observed by Landin *et al.*,[8] as previously discussed. To simplify the model, we have neglected the transfer paths that would include this large energy barrier in the hypothesis (b) framework, as we did for the carrier escape toward the barriers or from the QD's to the WL. The t_{3i} coefficients are thus assumed to be independent of temperature, and zero in the case of large dots.

We therefore obtain the same equation as in model (a), but with $R_{Ei} = 0$. Emission thus occurs only at energy E_i^{GS}:

$$i_{Qi}^{(b)} = R_{Qi}n_{Qi} = \frac{\frac{i_{Q0i}}{1+A_i}}{1+c_{Qi}\exp(-\Delta\text{hh}_i/k_BT)} \times\left[1+A_i\frac{1+D\exp(-E_{a1}/k_BT)}{1+c_W\exp(-E_{a1}/k_BT)}\right]. \quad (4)$$

For the thicker dots, we assume $A_i = t_{3i} = 0$, so Eq. (4) reduces to Eq. (1), with Δhh_i as the activation energy.

We can now fit the temperature behavior of the PL for the single-layer sample using Eqs. (2) and (4). The values of c_W and E_{a1} were found previously (see C_{WL} and $E_{a\mathrm{WL}}$ in Table I) and the values of $\Delta \mathrm{hh}_i$ are calculated with our EFA model. This leaves three parameters to fit for each QD family curve containing an intensity rise, A_i, c_{Qi}, and D, and only one (c_{Qi}) for those corresponding to larger QD's, since then $A_i = 0$. Because Eq. (4) contains the product of A_i by $(1 + A_i)^{-1}$, any finite nonzero value for A_i results in an equivalent fit for the thinner QD curves. Therefore, the temperature evolution of the QD PL cannot provide information on the fraction $I_{QDi0}A_i/(1 + A_i)$ of carrier pairs populating the QD's that were initially captured by the WL at LT. However, we know from our single-layer experimental results at LT that T_1 is greater than T_2 and of the same order of magnitude, since the carriers initially captured by the WL contribute to emission from both the WL and the QD's and $(I_{\mathrm{WL0}})^{\mathrm{SL}} \approx (I_{\mathrm{QD0}})^{\mathrm{SL}}$. In addition, the value of D, which should be the same for all families, depends on the chosen values of A_i [the numerator exponential prefactor is $I_{\mathrm{QD}i0}A_i D/(1 + A_i)$]. We can only determine a minimum value for D, which is greater than c_W [$c_W \equiv (T_3 + N_W)/(T_3 + L + N_W)D$]. Note that assuming $A_i \neq 0$ for large families leads to $D = c_W$, in contradiction with the latest condition. The c_{Qi} fits are nevertheless robust, since they do not depend on the values of A_i and D.[39]

In summary, the temperature behavior of the luminescence from the single-layer sample can be explained by the combined effects of the thermalization of the holes to the hh2 nearly dark state and of an efficient transfer of the carriers initially captured by the WL only toward the thinner QD's.

For multilayers (N layers), neglecting the coupling between the different layers, we have $I_{\mathrm{WL}} = \sum_{j=1}^{N} (I_W)_j$ and $I_{\mathrm{QD}} = \sum_i [\sum_{j=1}^{N} (i_{Qi}^{(b)})_j] = \sum_i I_{Qi} = \sum_{j=1}^{N} [(i_{\mathrm{QD}})_j]$. We have found for the WL's the same activation energy for the SL and the BL samples (see Table I). In fact, the C_{WL} and $E_{a\mathrm{WL}}$ values found for the BL sample are representative mainly of the first deposited WL for the BL sample, since $(I_{\mathrm{WL}})^{\mathrm{BL}} \approx (I_W)_1^{\mathrm{BL}}$. Indeed, we have discussed earlier that the thinning of the upper WL's in thin spacer multilayers should considerably reduce the number of 2D islands that can trap the carriers.

We will therefore consider that $(L)_j$ is negligible for $j \geqslant 2$ in what follows, so $I_{\mathrm{WL}} \approx (I_W)_1$. This implies $(D)_j \approx (C)_j$ and $(c_W)_1 \approx C_{\mathrm{WL}}$. Assuming in addition that $(c_{Qi})_1 \approx \cdots \approx (c_{Qi})_N \approx \langle (c_{Qi})_j \rangle \approx C_{Qi}$, we obtain, for each subset of QD's in multilayers,

$$
\begin{aligned}
I_{Qi} &\approx \frac{\frac{(i_{Q0i})_1}{1+(A_i)_1} + \sum_{j=2}^{N} (i_{Q0i})_j}{1 + C_{Qi}\exp(-\Delta \mathrm{hh}_i/k_B T)} \\
&\quad \times \left[1 + \frac{(A_i)_1 (i_{Q0i})_1}{(i_{Q0i})_1 + [1 + (A_i)_1]\sum_{j=2}^{N} (i_{Q0i})_j} \right. \\
&\quad \left. \times \frac{1 + (D)_1 \exp(-E_{a1}/k_B T)}{1 + C_{\mathrm{WL}} \exp(-E_{a1}/k_B T)}\right] \\
&\approx \frac{\frac{I_{Q0i}}{1+A\prime}}{1 + C_{Qi}\exp(-\Delta \mathrm{hh}_i/k_B T)} \\
&\quad \times \left[1 + A\prime \frac{1 + (D)_1 \exp(-E_{a1}/k_B T)}{1 + C_{\mathrm{WL}} \exp(-E_{a1}/k_B T)}\right]. \qquad (5)
\end{aligned}
$$

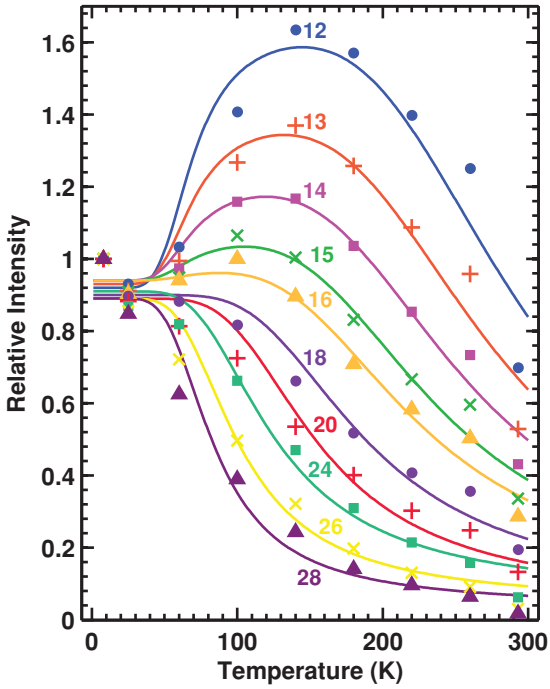

FIG. 8. (Color online) Data from Fig. 6(b) for the bilayer sample reported on a relative intensity scale and their fit using Eq. (5). The family index is given next to each curve.

Equation (5) thus reduces to Eq. (4) if the $(c_{Qi})_j$ coefficients are of the same order from one layer to the next. This implies no drastic increase of nonradiative recombination inside the dots through the multilayer, which is reasonable considering our results (important contribution from the upper layers to the QD spectra).

As shown in Fig. 8, which presents the results using a relative scale for the different QD families for the bilayer sample, Eq. (5) fits the multilayer data quite well. The temperature behavior of our multilayer luminescence can therefore be explained without considering any coupling between the QD layers. We have used the same activation energy E_{a1} for the escape of the carriers out of the 2D islands of the WL for all samples, i.e., $(E_{a1})^{\mathrm{SL}} = 27$ meV. It was verified that the C_{Qi} coefficients found for the multilayers are relatively close to those for the single-layer sample. Since there is no signal from the WL for the four-layer (FL) sample, we had one more parameter to fit with the QD-family curves: C_{WL}. The best fits are obtained for $(C_{\mathrm{WL}})^{\mathrm{FL}} = 35$. The fact that the total intensity is only 2.4 times that of the single layer for this four-period sample can be explained by an increase of the recombination rate N_B in the barriers (I_{QD0} is reduced, but the C_{Qi} coefficients are not affected).

So, in contrast with the C_{Qi} coefficients, the C_{WL} parameter seems to be nearly inversely proportional to the number of layer deposited for those thin-spacer layers. In fact, the ratios $(C_{\mathrm{WL}})^{\mathrm{SL}}/(C_{\mathrm{WL}})^{\mathrm{BL}}$ and $(I_{\mathrm{WL0}})^{\mathrm{SL}}/(I_{W0})^{\mathrm{BL}}$ are both slightly over 2. Since our results show that $T_3 \gg N_W$ (most of the carriers lost by the WL's are captured by the QD's), the decrease of these two parameters by a factor of 2 when adding a layer must arise from the $N_T{}^{-1}$ term in Eqs. (2) and (4). This indicates

that the close stacking of QD layers mostly deteriorates the luminescence from the WL's and has a negligible impact on the competition between the radiative and nonradiative processes inside the SK QD's. The high shift of the remaining signal from the first wetting layer of the BL as compared with that from the WL of the single-layer sample could imply that those recombination centers induce a defect energy level in the InP gap that is easily accessible to the carriers (to the excitons or to either one of the individual carriers) localized in the nanostructures emitting at around 1.2 eV and up.

Overall, the analysis of the PL spectra from the multilayer samples reveals that the progressive thinning of WL's in closely stacked layers strongly reduces the luminescence from the upper WL's and leads to an increase of the carrier transfers to the smaller QD's at low temperature. In addition, the important deformation in the thin spacers causes a sublinear dependence of the total intensity as a function of the number of layers. This mostly affects the PL intensity arising from the WL's, which decreases as more layers are stacked.

Finally, the temperature behavior of the multilayers can be described using the same model as for the single-layer sample. An electronic coupling between dots of different layers should imply additional coupled states accessible for the redistribution of carriers confined in interacting QD's as the temperature increases. Yet no other activated process could be observed when closely stacking the InAs(P) layers, besides the population of the nearly dark state also occurring in the single-layer sample. The interdot interaction is thus too weak to have a significant impact on the carrier dynamics.

V. CONCLUSION

We have demonstrated that the carrier dynamics and the temperature dependence of the emission from InAs QD multilayers in InP depend strongly on the QD height. We have observed that for thick InAs/InP QD's emitting in the 0.6–0.8 eV spectral region, the emission from the thinner dots is favored as the temperature is increased, and that the overall temperature-induced redshift of the PL is reduced as compared to that for individual QD's. The treatment of the emission intensity as separate contributions from the different families of QD's of the same height has enabled us to explain our results using the thermalization of the holes to their first excited state (hh2) (from which recombination with electrons in their ground state is weak) as the main path for the activated nonradiative recombination of the carriers. The rapid quenching with temperature of the luminescence from large dots emitting under 0.65 eV at low temperature is consistent with the proximity of this nearly dark state. In addition, the carriers captured by the WL's are efficiently transferred only to the smaller QD's emitting at ∼0.7 eV and up, probably due to the thinning of the surrounding WL during the ripening of the larger islands. This favors the emission from the smaller QD's when the increase in temperature allows the carriers' escape from the 2D islands of the WL.

Despite an ∼5-nm-thick spacer layer, the temperature dependence of the luminescence from our multilayers can be explained without including any electronic coupling between QD's of different layers, probably due to the deep confinement of the carriers in this type of relatively large nanostructures emitting below ∼0.8 eV. Still, stacking layers of vertically aligned QD's increases the transfer of the carriers captured by the second and subsequent WL's toward the QD's at low temperature. For applications, the barriers (spacers) should, however, be grown thicker than those in our samples to limit the strain-induced defects in the structure that weakens the PL intensity, but thin enough to stimulate the vertical organization of the islands.

ACKNOWLEDGMENTS

The authors acknowledge the help of G. Bentoumi for PL measurements and the technical assistance of J. Bouchard in the metal-organic vapor phase epitaxy laboratory of École Polytechnique de Montréal. This work was supported by the Natural Sciences and Engineering Research Council of Canada (NSERC) and the Canada Research Chair Program.

[1] S. Fafard, S. Raymond, G. Wang, R. Leon, D. Leonard, S. Charbonneau, J. L. Merz, P. M. Petroff, and J. E. Bowers, Surf. Sci. **361-362**, 778 (1996).

[2] Z. Y. Xu, Z. D. Lu, X. P. Yang, Z. L. Yuan, B. Z. Zheng, J. Z. Xu, W. K. Ge, Y. Wang, J. Wang, and L. L. Chang, Phys. Rev. B **54**, 11528 (1996).

[3] S. Sanguinetti, M. Henini, M. G. Alessi, M. Capizzi, P. Frigeri, and S. Franchi, Phys. Rev. B **60**, 8276 (1999).

[4] R. Heitz, I. Mukhametzhanov, A. Madhukar, A. Hoffmann, and D. Bimberg, J. Electron. Mater. **28**, 520 (1999).

[5] E. C. Le Ru, J. Fack, and R. Murray, Phys. Rev. B **67**, 245318 (2003).

[6] P. Dawson, O. Rubel, S. D. Baranovskii, K. Pierz, P. Thomas, and E. O. Gobel, Phys. Rev. B **72**, 235301 (2005).

[7] H. Marchand *et al.*, J. Electron. Mater. **26**, 1205 (1997).

[8] L. Landin *et al.*, Thin Solid Films **364**, 161 (2000).

[9] A. Lanacer, N. Shtinkov, P. Desjardins, R. A. Masut, and R. Leonelli, Semicond. Sci. Technol. **22**, 1282 (2007).

[10] B. Bansal, M. R. Gokhale, A. Bhattacharya, and B. M. Arora, J. Cryst. Growth **298**, 586 (2007).

[11] C. Dion, P. Desjardins, N. Shtinkov, M. D. Robertson, F. Schiettekatte, P. J. Poole, and S. Raymond, Phys. Rev. B **77**, 075338 (2008).

[12] G. Gélinas, A. Lanacer, R. Leonelli, R. A. Masut, and P. J. Poole, Phys. Rev. B **81**, 235426 (2010).

[13] B. Salem, J. Olivares, J. Brault, C. Monat, M. Gendry, G. Hollinger, H. Maaref, G. Guillot, and G. Bremond, Microelectron. J. **33**, 579 (2002).

[14] B. Salem, T. Benyattou, G. Guillot, C. Bru-Chevallier, G. Bremond, C. Monat, G. Hollinger, and M. Gendry, Phys. Rev. B **66**, 193305 (2002).

[15]H. Chouaib, N. Chauvin, C. Bru-Chevallier, C. Monat, P. Regreny, and M. Gendry, Appl. Surf. Sci. **253**, 90 (2006).
[16]S. Sanguinetti, M. Padovani, M. Gurioli, E. Grilli, M. Guzzi, A. Vinattieri, M. Colocci, P. Frigeri, and S. Franchi, Appl. Phys. Lett. **77**, 1307 (2000).
[17]J. J. Yoon *et al*., Physica E **26**, 207 (2005).
[18]Yu. I. Mazur, Zh. M. Wang, G. G. Tarasov, Vas. P. Kunets, G. J. Salamo, Z. Ya. Zhuchenko, and H. Kissel, J. Appl. Phys. **98**, 53515 (2005).
[19]P. Cova, R. A. Masut, J. F. Currie, A. Bensaada, R. Leonelli, C. Anh Tran, Can. J. Phys. **69**, 412 (1991).
[20]Q. Xie, A. Madhukar, P. Chen, and N. P. Kobayashi, Phys. Rev. Lett. **75**, 2542 (1995).
[21]G. Springholz, M. Pinczolits, P. Mayer, V. Holy, G. Bauer, H. H. Kang, and L. Salamanca-Riba, Phys. Rev. Lett. **84**, 4669 (2000).
[22]A. Lévesque, N. Shtinkov, R. A. Masut, and P. Desjardins, Phys. Rev. Lett. **100**, 046101 (2008).
[23]I. Vurgaftman, J. R. Meyer, and L. R. Ram-Mohan, J. Appl. Phys. **89**, 5815 (2001).
[24]Z. M. Fang, K. Y. Ma, D. H. Jaw, R. M. Cohen, and G. B. Stringfellow, J. Appl. Phys. **67**, 7034 (1990).
[25]G. Bacher, H. Schweizer, J. Kovac, A. Forchel, H. Nickel, W. Schlapp, and R. Losch, Phys. Rev. B **43**, 9312 (1991).
[26]E. M. Daly, T. J. Glynn, J. D. Lambkin, L. Considine, and S. Walsh, Phys. Rev. B **52**, 4696 (1995).
[27]N. Shtinkov, P. Desjardins, R. A. Masut, and S. J. Vlaev, Phys. Rev. B **70**, 155302 (2004).
[28]O. G. Schmidt, K. Eberl, O. Kienzle, F. Ernst, S. Christiansen, and H. P. Strunk, Mater. Sci. Eng. B **74**, 248 (2000).
[29]H. Folliot, S. Loualiche, B. Lambert, V. Drouot, and A. LeCorre, Phys. Rev. B **58**, 10700 (1998).
[30]G. L. Bir and G. Pikus, *Symmetry and Strain-Induced Effects in Semiconductors* (Wiley, New York, 1974).
[31]M. Beaudoin, A. Bensaada, R. Leonelli, P. Desjardins, R. A. Masut, L. Isnard, A. Chennouf, and G. L'Esperance, Phys. Rev. B **53**, 1990 (1996).
[32]C. Cornet, C. Levallois, P. Caroff, H. Folliot, C. Labbe, J. Even, A. Le Corre, S. Loualiche, M. Hayne, and V. V. Moshchalkov, Appl. Phys. Lett. **87**, 233111 (2005).
[33]Y.-G. Zhao, R. A. Masut, J. L. Brebner, C. A. Tran, and J. T. Graham, J. Appl. Phys. **76**, 5921 (1994).
[34]A. S. Jordan, J. Cryst. Growth **71**, 559 (1985).
[35]N. S. Orlova, Cryst. Res. Technol. **24**, 39 (1989).
[36]N. N. Sirota, A. M. Antyukhov, and A. A. Sidorov, Dokl. Akad. Nauk SSSR **277**, 1379 (1984) [Sov. Phys. Dokl. **29**, 662 (1984)].
[37]Z. Hang, H. Shen, and F. H. Pollak, Solid State Commun. **73**, 15 (1990).
[38]W. Seifert, N. Carlsson, M. Miller, M.-E. Pistol, L. Samuelson, and L. R. Wallenberg, Prog. Cryst. Growth Charact. Mater. **33**, 423 (1996).
[39]The fitted values of c_{Qi} increase monotonically between 18 for *f*26 and 172 for *f*12 for the single-layer sample.